Clinical Neurophysiology 132 (2021) 392–403

Contents lists available at ScienceDirect

Clinical Neurophysiology

journal homepage: www.elsevier.com/locate/clinph

Quantitative assessment of visual pathway function in blind retinitis pigmentosa patients

Minfang Zhang [1], Wangbin Ouyang [1], Hao Wang, Xiaohong Meng, Shiying Li *, Zheng Qin Yin *

Southwest Hospital/Southwest Eye Hospital, Third Military Medical University (Army Medical University), Chongqing 400038, PR China
Key Lab of Visual Damage and Regeneration & Restoration of Chongqing, Chongqing 400038, PR China

ARTICLE INFO

Article history:
Accepted 8 November 2020

Keywords:
Blind retinitis pigmentosa
Visual pathway function assessment
Visual evoked potential
Pupillary light response
Functional magnetic resonance imaging

HIGHLIGHTS

- Visual pathway function can be quantified in blind retinitis pigmentosa patients.
- Optical coherence tomography findings, visual evoked potentials, pupillary light responses and functional magnetic resonance imaging findings are appropriate objective, quantitative indicators.
- This study has clinical significance for predicting patient prognoses and the degree to which clinical treatments restore vision in patients with blindness associated with retinitis pigmentosa.

ABSTRACT

Objective: The current methods used to assess visual function in blind retinitis pigmentosa (RP) patients are mostly subjective. We aimed to identify effective, objective methods.
Methods: We enrolled patients diagnosed with blindness associated with RP; we finally selected 26 patients (51 eyes) with a visual field radius less than 10 degrees and divided them into the following 4 groups by best-corrected visual acuity (BCVA): group 1, no light perception (NLP, 4 eyes); group 2, light perception (LP, 12 eyes); group 3, hand movement or finger counting (faint form perception, FFP, 22 eyes); and group 4, BCVA from 0.1 to 0.8 (form perception, FP, 13 eyes). All patients underwent optometry, optical coherence tomography (OCT), color fundus photography, fundus autofluorescence (FAF), full field electroretinography (ffERG), pattern electroretinography (PERG), multifocal electroretinography (mf-ERG), pattern visual evoked potential (PVEP), flash visual evoked potential (FVEP), and pupillary light response (PLR) assessments. Five patients in groups 1, 2, and 3 (1, 2, and 2 subjects, respectively) underwent functional magnetic resonance imaging (fMRI) scans and were compared with five healthy subjects.
Results: The outer plexiform layer was thinner in group 1, and the outer nuclear layer was thinner in groups 1 and 2. The ffERG, PERG, and mf-ERG findings were unrecordable in all four groups. The P2 amplitude of the FVEP was significantly lower in groups 1 and 2, while the P100 amplitude of the PVEP was higher in groups 2, 3 and 4 than in group 1. After white- and blue-light stimuli, the PLR thresholds in the patients without form perception were significantly higher. The threshold of the PLR stimulated by blue and white light was negatively correlated with the amplitudes of P2 and P100. Moreover, the fMRI findings showed that some RP patients have significant visual cortex activation in response to certain types of stimulation. However, statistical analysis was not performed because of the small number of cases.
Conclusions: OCT, VEP, PLR and fMRI assessments can evaluate residual visual pathway function in blind RP patients.
Significance: Our study may have clinical significance for the potential prediction of RP patient prognoses and the effects after clinical trials.

* Corresponding authors at: Southwest Hospital/Southwest Eye Hospital, Third Military Medical University (Army Medical University), Chongqing 400038, PR China.
E-mail addresses: shiying_li@126.com (S. Li), qinzyin@aliyun.com (Z.Q. Yin).
[1] These authors contributed to the work equally and should be regarded as co-first authors.

https://doi.org/10.1016/j.clinph.2020.11.023
1388-2457/

1. Introduction

Retinitis pigmentosa (RP) is a severe hereditary disease that leads to progressive impairment of visual cells and photoreceptor cells. It has a worldwide incidence rate of approximately 1/3000–1/4000 (Fahim, 2018), and its clinical features include night blindness, tunnel vision, and osteocyte-like pigmentation on the retina. In the advanced stage of the disease, patients can become completely blind. The current treatments include pharmacological approaches, gene therapy, cell transplantation, retinal prostheses and optogenetics (Dias et al., 2018; Duebel et al., 2015; Klassen, 2016; Liu et al., 2017; Maguire et al., 2019; Miraldi Utz et al., 2018; Rachitskaya and Yuan, 2016; Russell et al., 2017; Verbakel et al., 2018). In both ongoing and completed human clinical trials, one of the major challenges is how to objectively assess the visual pathway function of blind RP patients before and after treatment (Dias et al., 2018, Klassen, 2016; Rachitskaya and Yuan, 2016). In a clinical trial aimed at treating Leber congenital amaurosis (LCA) caused by mutations in RPE65, the participants had visual acuity of 20/60 or worse or a visual field less than 20 degrees (Maguire et al., 2019; Russell et al., 2017). For retinal prostheses, such as the Argus II system, subjects whose visual acuity is light perception (LP) or no LP (NLP) are recruited (Rachitskaya and Yuan, 2016). For these subjects, conventional visual function examinations, such as visual acuity and visual field assessments, are unreliable and insensitive because of their poor vision and fixation (Jolly et al., 2019; Luo and da Cruz, 2016).

The International Classification of Diseases 11th Edition (ICD-11) defines blindness as a distance visual acuity worse than 3/60 or a visual field radius less than 10 degrees (Khoury et al., 2017), which is the blindness criterion in most jurisdictions. Physiological blindness usually refers to the loss of the entire visual fields, including LP and NLP. Researchers have used the multiluminance mobility test (MLMT) and full-field light sensitivity threshold testing (FST) to assess visual pathway function in the treatment of LCA (Maguire et al., 2019; Miraldi Utz et al., 2018). The square localization test, direction of motion test, letter recognition, real-world condition assessments and functional low-vision observer rated assessment (FLORA) have been used to assess visual pathway function in patients who received the Argus II retinal prosthesis system (Rachitskaya and Yuan, 2016). However, all of the above visual function tests are subjective. Objective testing to determine the functional capacity of the remaining retina in blind patients has not been fully established.

Functional magnetic resonance imaging (fMRI) is a noninvasive imaging technology for the detection of neuroactivity and depiction of brain function. Since it was invented in the early 1990s, it has played a vital role in understanding the brain and has been widely used in cognitive neuroscience and mental illness because of its superior temporal and spatial resolution (Amaro and Barker, 2006; Krueger and Granziera, 2012; Logothetis, 2008; Rosen and Savoy, 2012). The main principle of blood oxygen level dependent (BOLD) imaging is to detect changes in oxygen levels, which reveal neuronal activity, by detecting the paramagnetism of deoxyhemoglobin and diamagnetism of oxyhemoglobin (Buxton et al., 2014; Masamoto et al., 2008; Ogawa et al., 1990). In a narrow sense, fMRI refers to BOLD-fMRI. In ophthalmology, fMRI has been used to study visual cortex function in glaucoma (Chen et al., 2017; Frezzotti et al., 2014), amblyopia (Wang et al., 2017; Wang et al., 2012), optic neuritis (Finke et al., 2018; You et al., 2019) and RP (Ashtari et al., 2017; Dan et al., 2019; Masuda et al., 2010; Rita Machado et al., 2017; Yoshida et al., 2014). Thus, fMRI may be an appropriate method to evaluate residual visual pathway function in RP.

This study used patients with advanced or end-stage disease whose vision or visual field met the standard of blindness as research subjects and aimed to find the most valuable evaluation indicators by conducting a comprehensive examination of the visual structure and function. To the best of our knowledge, our study was the first to systematically assess the visual pathway function of RP patients from the retina to the optic nerve to the subcortical center to the visual cortex. We hope it can provide some objective information regarding the evaluation of residual visual function in blind patients. Such methods may also be useful to evaluate the recovery degree in blind patients who accept gene therapy or other treatments.

2. Methods

This was a prospective study of blind RP patients diagnosed by three senior ophthalmologists from the Southwest Hospital Eye Institute, Army Medical University, Chongqing, China, from January 2017 to December 2018. The study protocol was approved by the Institutional Review Board of the Army Medical University, Southwest Hospital (2017 scientific research No. 17) and was performed in accordance with the tenets of the Declaration of Helsinki.

2.1. Study population

The study included 26 patients with a diagnosis of blindness associated with RP. A total of 51 eyes were included; one eye was excluded because of poor cooperation. Five additional healthy volunteers were enrolled as controls for fMRI (Fig. 1). The diagnosis of blindness associated with RP was based on each person's medical history of nyctalopia, family history, characteristic fundus appearance of bone spicule pigment deposition in the retina, concentric reduction of the visual field, and markedly reduced a-wave and b-wave amplitudes on full field electroretinogram (ffERG). Other multimodal imaging techniques, such as optical coherence tomography (OCT), fundus autofluorescence (FAF), and fluorescein fundus angiography (FFA), were performed to confirm the diagnosis of RP. If the patients could not see the fixation when they were examined, we instructed them to look ahead and had a technician check the fixation to ensure it.

2.1.1. Inclusion criteria

a. Patients aged 18–60 years (inclusive).
b. Patients diagnosed with blindness associated with RP: The diagnosis of RP was performed as mentioned above, and either the best-corrected visual acuity (BCVA) of the study eyes was worse than 3/60 or the visual field radius was less than 10 degrees.
c. Patient history of night blindness of less than 30 years and patient history of central visual acuity loss of less than 10 years.

2.1.2. Exclusion criteria

a. The presence of any other eye diseases in the study eye that could cause visual impairment, including severe cataracts, glaucoma, retinal vascular occlusion, retinal detachment, macular holes, or vitreous macular traction.
b. Active inflammation in any eye, such as conjunctivitis, keratitis, scleritis, uveitis, or endophthalmitis.
c. History of intraocular surgery in the previous 6 months.
d. General conditions or treatments: history of stroke, coronary heart disease, angina pectoris, renal insufficiency requiring dialysis or kidney transplantation or allergy to fluorescein sodium.
e. Pregnancy.

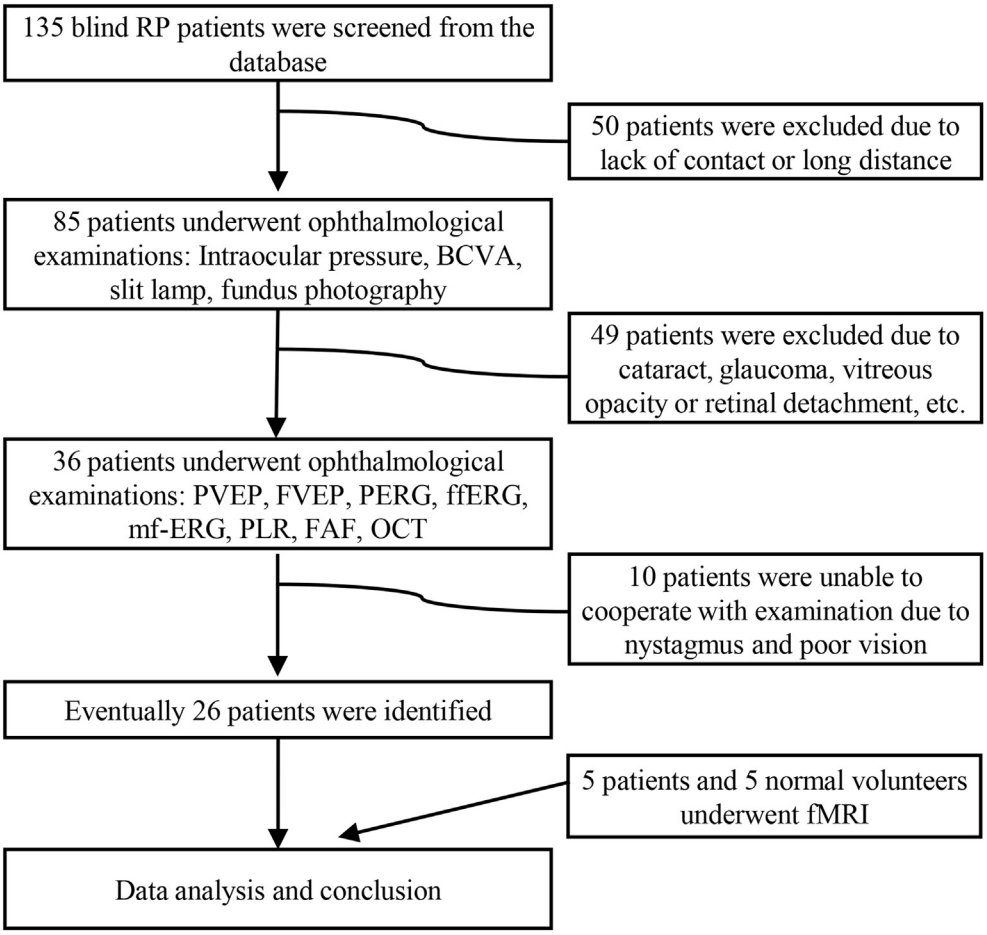

Fig. 1. Flow diagram of patient selection. RP: retinitis pigmentosa, BCVA: best-corrected visual acuity, PVEP: pattern visual evoked potential, FVEP: flash visual evoked potential, PERG: pattern electroretinogram, ffERG: full field electroretinogram, mf-ERG: multifocal electroretinogram, PLR: pupillary light response, FAF: fundus autofluorescence, OCT: optical coherence tomography, fMRI: functional magnetic resonance imaging.

2.2. Examination processes

2.2.1. Best-corrected visual acuity (BCVA) testing

The BCVA was examined with an autorefractor (NIDEK AR310, Japan) and a subjective refractometer (NIDEK RT-2100, Japan) at 5 m.

2.2.2. Color fundus photography (CFP)

CFP was used to observe retinal changes in RP. It was performed with a fundus camera (Kowa Nonmyd α-D, Japan). All images were acquired with 5-megapixel resolution and a 45° field.

2.2.3. Fundus autofluorescence (FAF)

A confocal scanning laser ophthalmoscope (Spectralis HRA +OCT; Heidelberg Engineering, Germany) was used to record FAF images and estimate retinal pigment epithelium (RPE) health. Excitation at 488 nm was used at 100% laser power and 95% detector sensitivity. All images were acquired with high resolution mode (55° field sampled onto 1536 × 1536 pixels). The manufacturer's automatic real-time (ART) feature with a 15-frame average was used whenever possible.

2.2.4. Spectral domain optical coherence tomography (SD-OCT)

SD-OCT was performed with the OCT-SLO Spectralis (HRA+OCT, Heidelberg Engineering, Germany) in study patients. OCT imaging was obtained by an 870 nm broadband superluminescent diode, which scans the retina at a speed of 40,000 A scans per second, with an optical axial depth resolution of 7 μm. The protocol included averaging a maximum of 10 OCT scans to improve the signal-to-noise ratio.

OCT was used to detect residual retinal layers and thickness in RP patients. The layers of the retina are defined as follows: macular retinal thickness (MRT, between the inner limiting membrane and the RPE); ganglion cell-inner plexiform layer (GCL-IPL, between the nerve fiber layer and the inner nuclear layer); inner nuclear layer (INL, between the inner plexiform layer and the outer plexiform layer); outer plexiform layer (OPL, between the inner nuclear layer and the outer nuclear layer); and outer nuclear layer (ONL, between the outer plexiform layer and the outer limiting membrane). The thicknesses of five points (macular center, macular center nasal 500 μm, macular center nasal 1000 μm, macular center temporal 500 μm and macular center temporal 1000 μm) were measured for the MRT, and four points (excluding the macular center) were measured for the GCL-IPL, INL, OPL and ONL.

2.2.5. Clinical visual electrophysiology

These measurements included ffERG, pattern electroretinography (PERG), multifocal electroretinography (mf-ERG), pattern visual evoked potential (PVEP) and flash visual evoked potential (FVEP) assessments. All followed the standards of the International Society for Clinical Electrophysiology of Vision (ISCEV).

ffERG (Espion system, Diagnosis LLC, Lowell, MA, U.S.A.) readings were recorded from both eyes with corneal electrodes. Six responses based on the adaptation state of the eye and the flash

strength were recorded: (1) dark-adapted 0.01 ERG; (2) dark-adapted 3.0 ERG; (3) dark-adapted 3.0 oscillatory potentials; (4) dark-adapted 10.0 ERG; (5) light-adapted 3.0 ERG; and (6) light-adapted 30 Hz flicker ERG.

PERG was recorded with an Espion E2 visual electrophysiological system (Diagnosys LLC, Lowell, MA, U.S.A.). A black and white reversing checkerboard was used as the stimulus. The width of the single checks (check size) for PERG was 1°. A reversal rate of 4.0 reversals per second (rps) (corresponding to 2.0 Hz) was used to obtain the standard transient PERG. The patients were directed to look straight ahead if they could not stare at the fixation center of the screen during PERG.

The mf-ERG technique uses a BA corneal electrode to record the electrophysiological response of the local area of the retina. A Veris system (Electro-Diagnostic Imaging, Inc., Burlingame, CA, U.S.A.) was used to record the mf-ERG response, and the patients' fixation was monitored by the fundus camera inside the machine.

The PVEP and FVEP were examined using a visual electrophysiological system (Espion E2 Diagnosis, U.S.A.). The PVEP was elicited by 1-degree and 0.25-degree checkerboard stimuli. The FVEP was elicited by a flash strength (duration of 5 ms) subtending a visual field of at least 20°. The recording electrode placement position was 2–3 cm on the occipital trochanter, the reference electrode placement position was the forehead center, and the ground electrode placement position was the earlobe. The FVEP was recorded in the order of right eye and left eye, and the eye not being tested was covered. The patients were directed to look straight ahead if they could not stare at the fixation center of the screen in PVEP.

2.2.6. Pupillary light response (PLR)

Pupillometry was checked with the French Metrovision company's visual surveillance system. The maximum flash stimulus intensity was 150 cd/m^2, the maximum background brightness was 2000 cd/m^2, and the infrared camera refresh rate was 200 Hz. The subjects rested quietly for 5 minutes in a dark room, sat down, and placed their eyes in front of the eyepiece. White light and blue light were used as the stimuli, and brightness values of 1.0×10^{-3}, 1.0×10^{-2}, 1.0×10^{-1}, 1.0×10^{0}, $1.0 \times 10^{0.5}$, 1.0×10^{1}, and $1.0 \times 10^{1.5}$ cd/m^2 were used for stimulation. The stimulation time was 1 s, and the stimulation recording period was 7.5 s. The right eye was stimulated first, and then, the left eye was stimulated.

We defined the PLR threshold as the brightness at the first pupil contraction when patients were exposed to light stimuli. D_0 was the patient's initial pupil diameter without stimuli, and D_1 was the patient's smallest pupil diameter after stimulation in the same period. Then, the relative pupillary constriction (RPC) was equal to $(D_0\text{-}D_1)/D_0$.

2.2.7. Functional magnetic resonance imaging (fMRI)

2.2.7.1. Participants. Ten individuals participated in this study: five with RP and five normal control (NC) volunteers. The RP participants included one patient from group 1, two patients from group 2 and two patients from group 3. All NC volunteers had no refraction or refraction diopter < -6 D (BCVA $\geq$ 1.0) or other ocular diseases, such as cataracts, glaucoma, optic neuritis, and retinal degeneration. All the participants were right-handed.

2.2.7.2. MRI parameters. A 3-T scanner (Magnetom TrioTim, Siemens AG, Germany) in the Southwest Hospital Radiology Department was used to collect images. The whole-brain T1-weighted images were collected with the following parameters: $1 \times 1 \times 1$ mm^3 voxel size, 2 s repetition time (TR), 2.5 ms echo time (TE), 9° flip angle (FA), and 256×256 mm^2 field of view (FOV); 176 slices were acquired from each participant. The functional images consisting of echo planar imaging (EPI) were acquired with the following parameters: $3 \times 3 \times 3$ mm^3 voxel size, 2 s TR, 30 ms TE, 90° FA, 192×192 mm^2 FOV, 36 slices, and 64×64 imaging matrix.

2.2.7.3. MRI stimuli and experimental design. Each subject underwent four complete scans with the Visual Stimulation System for fMRI assembled at Shenzhen Sinorad Medical Electronics Inc. Each scan included six repeated blocks, and each block lasted one minute and was composed of two conditions: first, the black condition, which presented complete darkness lasting 30 s, and then, 30 s of light. We used white light stimulation because such stimulation could activate all types of photoreceptor cells. In addition, blue light was selected because residual photoreceptors are more sensitive to blue light. Four different types of light corresponding to four different types of stimuli were used: white flashes, blue flashes, white-black reversing checkerboard (white checkerboard) and blue-black reversing checkerboard (blue checkerboard). The stimulus programs were executed by E-prime 2.0 (Psychology Software Tools, Inc). The stimulus flickering frequency was 1 Hz (Fox and Raichle, 1984, 1985; Spitschan et al., 2016; Thomas and Menon, 1998). The stimuli were presented binocularly with refraction correction by MRI-compatible goggles.

2.2.7.4. MRI data processing. All preprocessing was implemented using the toolbox for Data Processing and Analysis of Brain Imaging (DPABI (Yan et al., 2016), which is based on Statistical Parametric Mapping (SPM 12) and executed in MATLAB 2013b (MathWorks, Natick, Massachusetts, U.S.A.). The processing steps were as follows: 1) All raw images were converted from DICOM format to NIfTI format. 2) All functional images (180) were realigned to eliminate the effect of head motion, and subjects whose head movement exceeded 1 mm or rotation exceeded 1 degree were excluded from subsequent analysis. 3) The T1-weighted structural images were registered to the mean function images, and the normalized data were resliced at a resolution of $3 \times 3 \times 3$ mm^3. 4) Smooth (FWHM = 8 mm) was used to reduce the noise effect.

2.2.7.5. MRI data analysis. We used a general linear model (GLM) to analyze the preprocessed data and used a box-car regressor corresponding to the light stimulation blocks. The regression factor was

Table 1
Baseline demographics of all RP patients' eyes.

	Group 1	Group 2	Group 3	Group 4
Eyes/patients	4/3	12/9	22/15	13/9
Sex (male/female)	2/2	10/2	9/13	6/7
Age range (avg ± STD)	33–55 (49.25 ± 10.84)	41–56 (44.58 ± 10.90)	25–56 (45.14 ± 10.80)	29–56 (45.06 ± 9.45)
History of night blindness (years)	13.50 ± 7.51	18.58 ± 8.50	20.73 ± 7.39	24.64 ± 6.74
History of central visual acuity loss (years)	10.00 ± 5.77	11.17 ± 6.77	9.14 ± 5.28	11.11 ± 8.84
BCVA result	NLP	LP	HM or CF	0.1–0.8
Visual field radius	0°	0°	0°	<10°

NLP: no light perception, LP: light perception, HM: hand movement, CF: counting finger, BCVA: best-corrected visual acuity.

convolved with the canonical hemodynamic response function (HRF) and compared with the dark blocks. The contrast images were the stimuli tasks with dark-condition subtraction.

The settings of SPM in model specification were as follows: The units for design chose scans. The interscan interval was the repetition time equal to 2 s. The microtime resolution was

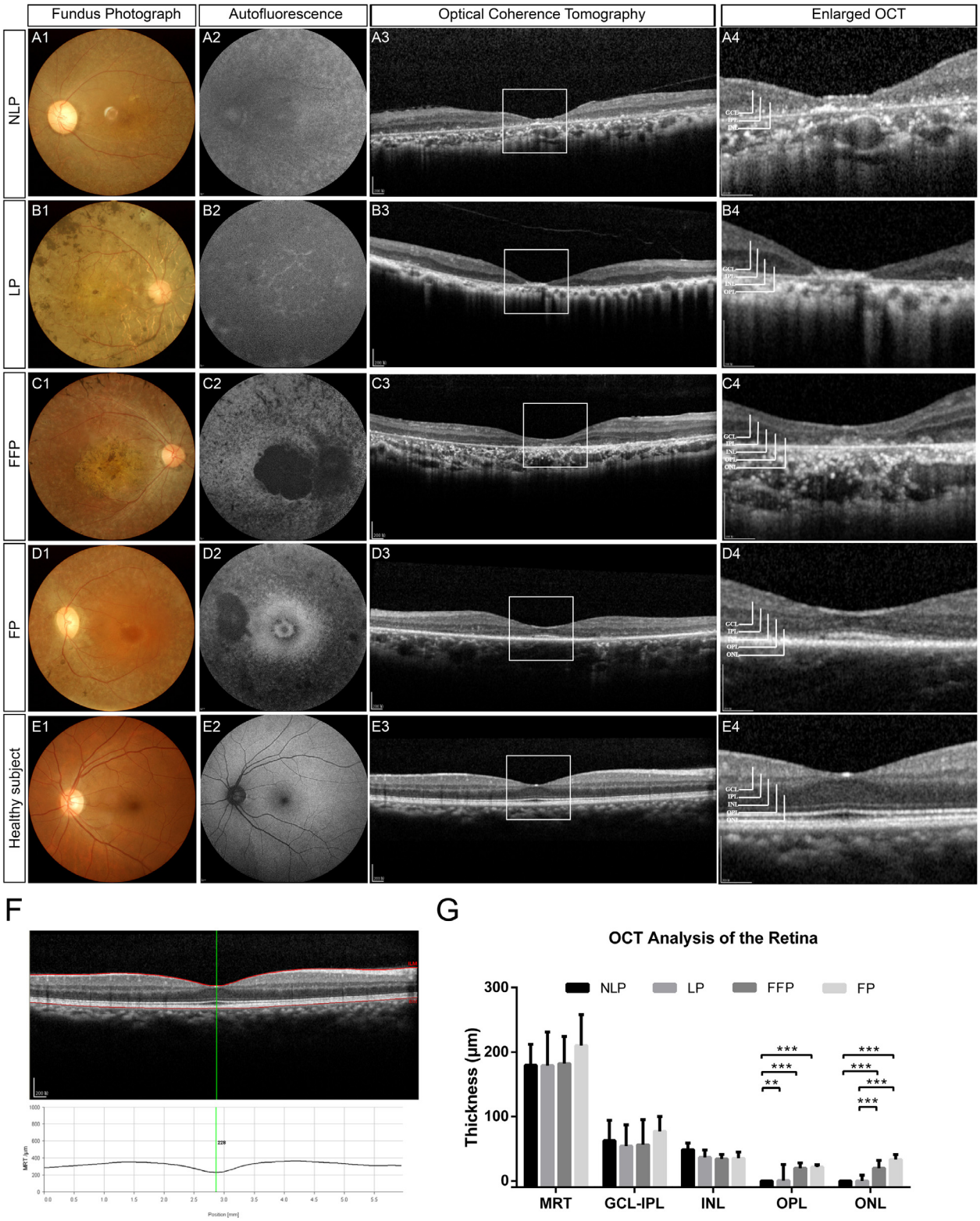

Fig. 2. Five groups' representative multimodal retinal imaging and OCT analysis of retinal thickness. (A-E) Subjects are ranked along the y-axis in ascending order of severity of visual acuity, and different examinations are shown along the x-axis. (F) An example measurement of MRT thickness. (G) Statistical analysis of the retinal layer thickness of different eyes among RP patients (NLP [N = 4], LP [N = 10], FFP [N = 18], FP [N = 11], MRT [H = 6.924, $P = 0.074$], GCL-IPL [H = 5.304, $P = 0.151$], INL [H = 3.814, $P = 0.282$], OPL [H = 38.086, $P < 0.001$], ONL [H = 63.114, $P < 0.001$], Kruskal-Wallis test). Interquartile ranges are shown with error bars. **P < 0.01, ***P < 0.001. NLP: no light perception, LP: light perception, FFP: faint form perception, FP: form perception, MRT: macular retinal thickness, GCL-IPL: ganglion cell layer-inner plexiform layer, INL: inner nuclear layer, OPL: outer plexiform layer, ONL: outer nuclear layer, OCT: optical coherence tomography.

the number of slices equal to 36, and the microtime onset was the reference slice's scan sequence equal to 18. As we described earlier, each scan included 6 repeated blocks, and each block was composed of dark conditions and light conditions. Each condition lasted 30 s, and 180 images were acquired in each run over the course of 6 minutes. Each participant completed 4 runs (white flashes, blue flashes, white checkerboard, blue checkerboard). We used a box-car regressor corresponding to the light stimulation blocks. The basis function chose the canonical HRF. A one-lag autoregression (AR (1)) model was used to correct for serial autocorrelations.

After first-level analysis for each participant, second-level analysis was run using a one-sample t-test in all groups. The peak-level topological false discovery rate (FDR) correction was used to correct multiple comparisons. The BrainNetViewer (https://www.nitrc.org/projects/bnv) toolbox was selected to show the activation maps of the visual cortex.

2.3. Other relevant variables

We asked about the patients' professions, living habits, including smoking history and drinking history, and some physical indicators, such as weight and height. There was no evidence that these factors were related to the progression of the disease.

2.4. Statistical analysis

According to their BCVA values, the study eyes were divided into four groups. The BCVAs of these four groups were NLP (4 eyes), LP (12 eyes), hand movement or counting fingers (faint form perception, FFP, 22 eyes) and 0.1–0.8 (form perception, FP, 13 eyes).

We used IBM SPSS Statistics, version 22 (IBM Corporation, U.S.A.) to perform the statistical analysis. Normality was verified first by the Shapiro-Wilk test. For data with a normal distribution, an independent-samples t-test or analysis of variance (ANOVA) was performed. Otherwise, nonparametric methods, including the Mann-Whitney and Kruskal-Wallis tests, were applied. The post hoc analysis was Bonferroni corrected. The method to analyze the correlation between the threshold of the PLR and the amplitude of the VEP was Spearman rank correlation analysis. Statistical significance was defined as P values < 0.05.

3. Results

3.1. Study population

A total of 51 eyes from 26 patients were included in this study. The patients were divided into four groups based on their BCVA results. The numbers of eyes in groups 1, 2, 3, and 4 were 4 eyes (7.8%), 12 eyes (23.5%), 22 eyes (43.1%) and 13 eyes (25.5%), respectively. The average RP patient ages were 49.25 ± 10.84, 44.58 ± 10.90, 45.14 ± 10.80 and 45.06 ± 9.45 (F = 0.259, P = 0.855, ANOVA) years in groups 1, 2, 3, and 4, respectively. The demographics of the study participants are shown in Table 1.

3.2. OCT showed that structural differences and retinal function cannot be evaluated by ERG in blind RP patients

FAF showed lesions of the RPE; as the disease progressed, almost no viable RPE remained in groups 1 and 2. From the OCT images, we could see that the damaged retina became thinner. To confirm which layer was damaged, we performed partial magnification of the OCT image and measured the thickness of the retinal layer. The thicknesses of the MRT, OPL and ONL in the four RP groups were significantly lower than those in healthy subjects (MRT [H = 162.659, P < 0.001], OPL [H = 63.904, P < 0.001], ONL [H = 189.51, P < 0.001], Kruskal-Wallis test). The OPL and ONL in group 1 were absent. We found that the OPL thickness in group 1 (N = 4) was significantly lower than that in groups 2 (N = 10), 3 (N = 18), and 4 (N = 11; P < 0.01, P < 0.001, and P < 0.001, respectively; Kruskal-Wallis test). The ONL in group 2 (N = 10) was significantly thinner than those in groups 3 (N = 18) and 4 (N = 11; P < 0.001 vs. P < 0.001; Kruskal-Wallis test) and that in group 2 (N = 10) was also significantly thinner than those in groups 3 (N = 18) and 4 (N = 11; P < 0.001 vs. P < 0.001; Kruskal-Wallis test). There was no significant difference in the MRT thickness (H = 6.924, P = 0.074, Kruskal-Wallis test), GCL-IPL (H = 5.304, P = 0.151; Kruskal-Wallis test) or INL (H = 3.814, P = 0.282, Kruskal-Wallis test) among the four RP groups (Fig. 2).

To evaluate the residual retinal function of RP patients, we performed a full examination with ERG techniques, including ffERG, PERG and mf-ERG. However, ffERG, PERG and mf-ERG were unrecordable in all cases under the ISCEV standard conditions (Fig. 3).

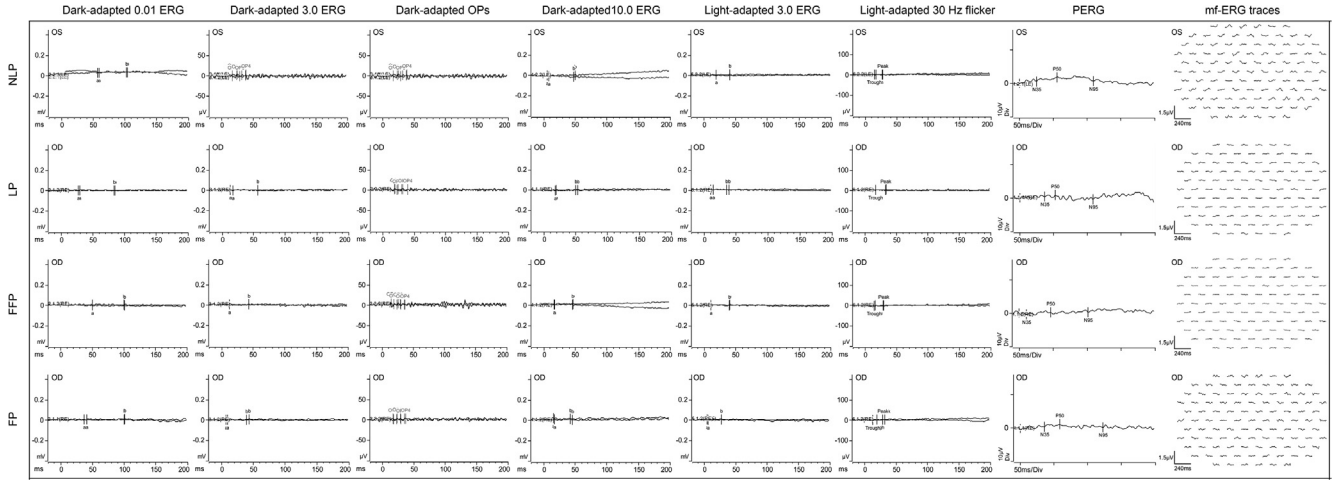

Fig. 3. Group comparisons of ERG (ffERG, PERG, and mf-ERG) among the four RP groups in accordance with the ISCEV standard. No meaningful waves were recorded. RP: retinitis pigmentosa, PERG: pattern electroretinogram, ffERG: full field electroretinogram, mf-ERG: multifocal electroretinogram, NLP: no light perception, LP: light perception, FFP: faint form perception, FP: form perception, ISCEV: International Society for Clinical Electrophysiology of Vision, OD: oculus dexter, OS: oculus sinister.

3.3. Examination of the optic nerve and subcortical nuclei can reflect RP patients' visual function

Based on the FVEP waves of the four groups, we noted that the overall visual acuity was poor, and the P2 wave amplitude was low. In groups 1, 2, 3, and 4, the P2 amplitudes were 0.34 (0.62) μV, 2.03 (0.83) μV, 3.07 (3.57) μV, and 6.71 (8.34) μV, respectively, and the P2 peak times were 115.25 (24.38) ms, 104.50 (25.13) ms, 103.75 (17.38) ms, and 121.50 (42.25) ms, respectively. The P100 amplitudes were 0.60 (0.98) μV, 0.73 (1.19) μV, 1.44 (1.61) μV, and 3.52 (3.07) μV in groups 1, 2, 3, and 4, respectively, and the P100 peak times were 105.25 (32.38) ms, 109.00 (19.88) ms, 109.00

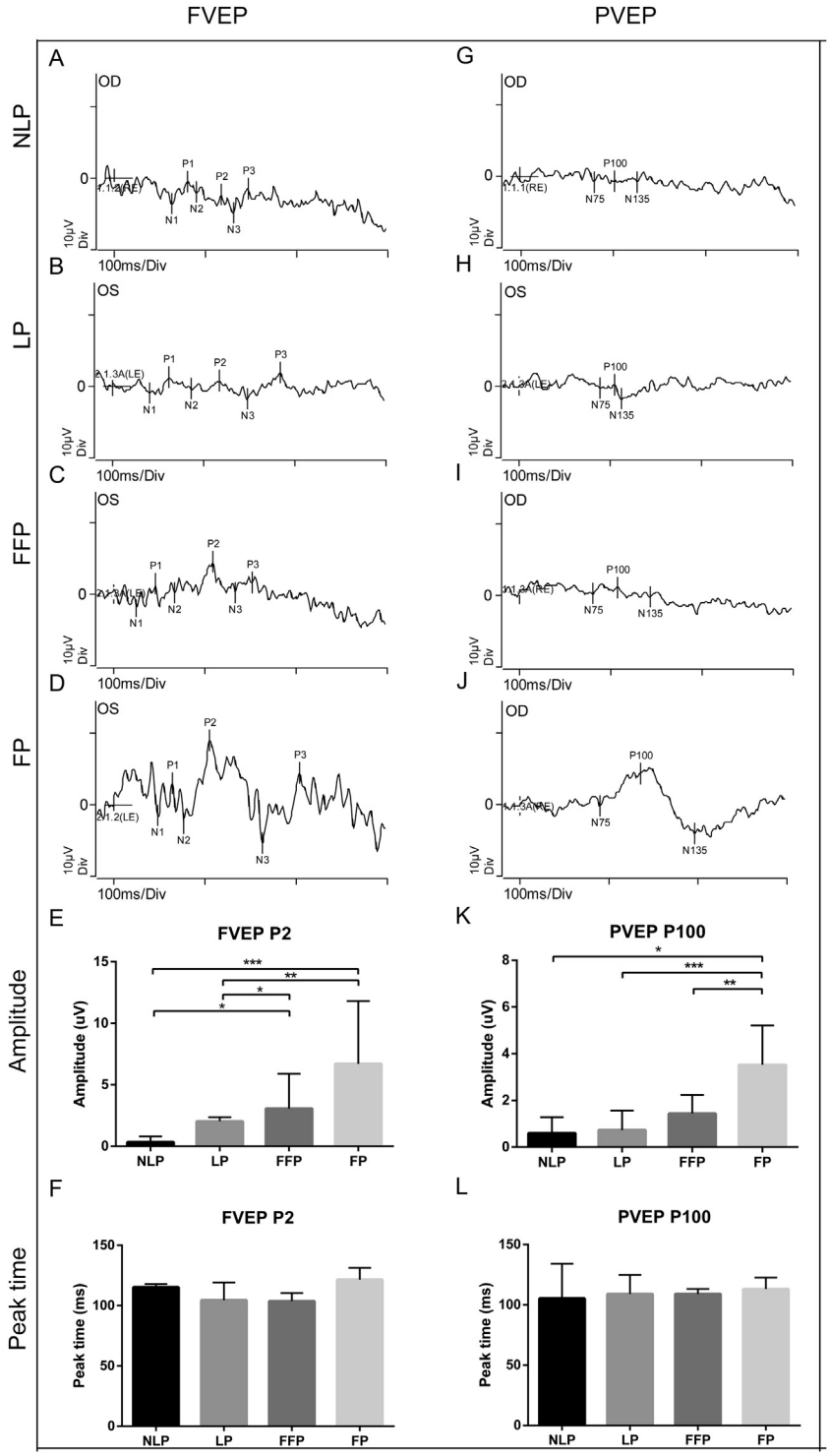

Fig. 4. Comparison of FVEP and PVEP results among RP patient eyes (NLP [N = 4], LP [N = 12], FFP [N = 22], FP [N = 13]). (A-F) Representation of the FVEP waves of the four RP groups and statistical analysis of the amplitude and peak time of the FVEP P2 wave (amplitude [H = 23.793, $P < 0.001$], peak time [H = 1.435, $P = 0.697$], Kruskal-Wallis test). (G-L) PVEP P100 wave responses in the four RP groups. The amplitude and peak time were analyzed (amplitude [H = 20.421, $P < 0.001$] and peak time [H = 4.002, $P = 0.261$], Kruskal-Wallis test). Interquartile ranges are shown with error bars. * $P < 0.05$, ** $P < 0.01$, *** $P < 0.001$. NLP: no light perception, LP: light perception, FFP: faint form perception, FP: form perception, FVEP: flash visual evoked potential, PVEP: pattern visual evoked potential, RP: retinitis pigmentosa, OD: oculus dexter, OS: oculus sinister.

(7.88) ms, and 113.00 (14.25) ms, respectively. The P2 amplitudes in group 1 (N = 4) and group 2 (N = 12) were significantly lower than those in group 3 (N = 22, $P < 0.05$, $P < 0.05$, Kruskal-Wallis test) and group 4 (N = 13, $P < 0.01$, $P < 0.001$, Kruskal-Wallis test). In addition, the P100 amplitudes in groups 1 (N = 4), 2 (N = 12), and 3 (N = 22) were significantly lower than those in group 4 (N = 13, $P < 0.01$, $P < 0.001$, $P < 0.01$, Kruskal-Wallis test). Neither the P2 nor the P100 wave peak time was significantly different among the four groups (H = 1.435, $P = 0.697$, H = 4.002, $P = 0.261$, Kruskal-Wallis test) (Fig. 4).

We calculated the threshold and RPC of all patients under white- and blue-light stimuli. Because of poor cooperation, in the condition of white-light stimuli, six patients (ten eyes) were excluded, and in the condition of blue-light stimuli, two patients (two eyes) were excluded. Thus, the sample sizes were 3 (group 1), 8 (group 2), 18 (group 3), and 12 (group 4) eyes for white-light stimuli and 4, 11, 21, and 13 eyes in groups 1, 2, 3, and 4, respectively, for blue-light stimuli. The PLR thresholds in group 1 and group 2 were significantly higher than those in group 3 ($P < 0.05$, $P < 0.01$, Kruskal-Wallis test) and group 4 ($P < 0.01$, $P < 0.01$, Kruskal-Wallis test) under the white- and blue-light stimuli. No significant difference in RPC was observed among the four groups under either white- (H = 2.372, $P = 0.499$, Kruskal-Wallis test) or blue-light stimuli (H = 6.442, $P = 0.092$, Kruskal-Wallis test) (Fig. 5).

Due to the similarity of the VEP and PLR results, we performed Spearman rank correlation analysis to explore the correlation between the threshold of the PLR and the amplitude of the VEP. We found that for subjects under white-light stimuli, the amplitude of P2 had a negative correlation with the threshold of the PLR (r = −0.435, $P = 0.002$). The amplitude of P100 also had a negative correlation with the PLR threshold under white-light stimulus (r = −0.435, $P = 0.003$). For patients under blue-light stimuli, the amplitude of P2 had a negative correlation with the PLR (r = −0.425, $P = 0.006$). Similarly, the correlation between the amplitude of P2 and the PLR threshold under a blue-light stimulus was negative (r = −0.432, $P = 0.007$) (Fig. 6).

3.4. Visual cortex activation detected by fMRI may be a direction for functional testing of RP patients in the future

Five RP patients underwent fMRI examinations and were designated PAT1 to PAT5. Another five volunteers (NC1- NC5) underwent fMRI as healthy controls. All ten subjects' ocular characteristics are displayed in Table 2.

We asked the patients whether they could feel the stimulation during the image acquisition, and all patients, except for PAT1, reported feeling the stimulation. Fig. 7 shows that some types of stimulation could activate the visual cortex of RP patients. The NLP group showed no significant activation. The HM group showed significant activation under four stimulus conditions. In the LP group, white flashes of light could not activate the visual cortex, but other types of light stimuli could activate it. However, no statistical analyses were performed due to the small number of cases. We cannot determine who had stronger activation (Fig. 7).

4. Discussion

Our study found that OCT, VEP, PLR and fMRI assessments could detect visual pathway function in blind RP patients to some extent. These methods consistently showed that patients with a BCVA indicating NLP or LP had poorer visual function than those with FP or even FFP.

In RP patients, retinal degeneration first appears as rod photoreceptor damage. With the advancement of the disease, cone

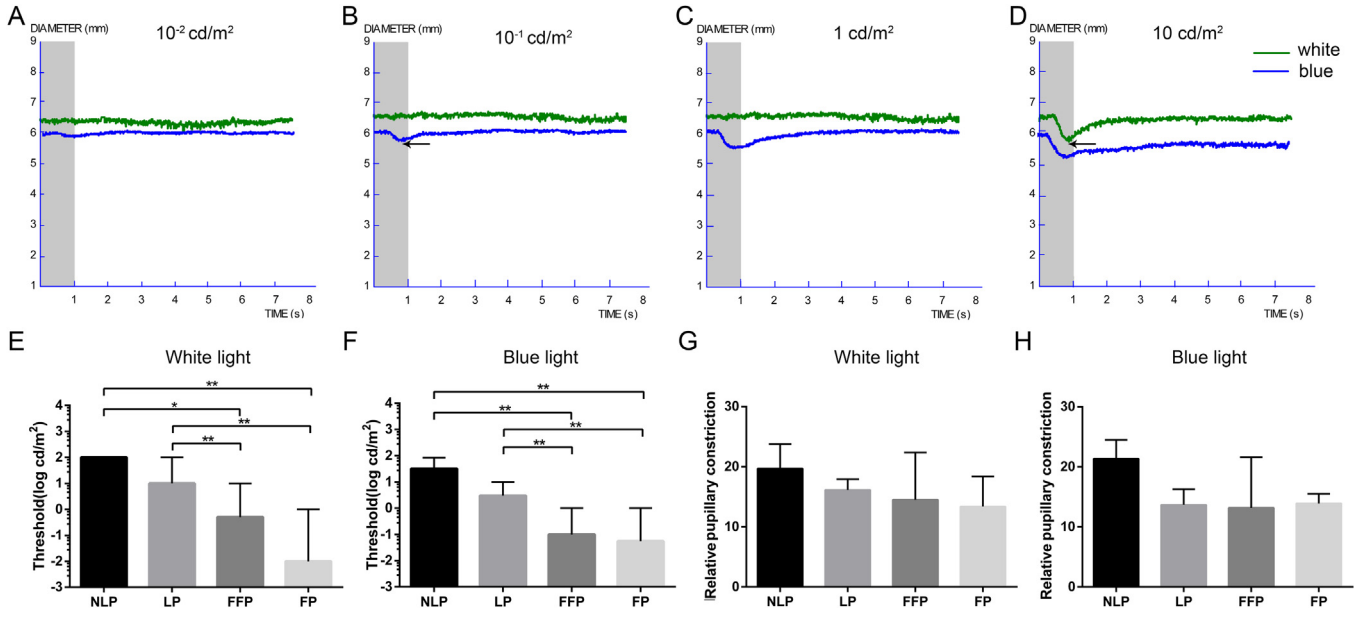

Fig. 5. PLR results of RP patients with white- and blue-light stimuli. (A-D) The PLR waves of the left eyes of a 29-year-old RP patient under white-light stimuli of different brightnesses (1×10^{-2} cd/m^2, 1×10^{-1} cd/m^2, 1 cd/m^2, 10 cd/m^2) are shown by the green curve. The PLR waves of the right eyes of a 30-year-old RP patient under blue-light stimuli of different brightnesses (1×10^{-2} cd/m^2, 1×10^{-1} cd/m^2, 1 cd/m^2, 10 cd/m^2) are shown by the blue curve. The trough of the curve represents the contraction of the pupil. (B) Noting the trough of the blue curve (black arrow), we defined the brightness when the first pupil contraction appeared under the stimuli as the threshold, so the threshold of this condition was 1×10^{-1} cd/m^2. (D) Similarly, 10 cd/m^2 was considered a threshold. (E-H) Statistical analysis of the PLR threshold (white [H = 21.828, $P < 0.001$], blue [H = 24.007, $P < 0.001$], Kruskal-Wallis test) and RPC (white [H = 2.372, $P = 0.499$], blue [H = 6.442, $P = 0.092$], Kruskal-Wallis test) under white- and blue-light stimuli. The sample sizes were 3 (NLP), 8 (LP), 18 (FFP), and 12 (FP) eyes for white-light stimuli and 4, 11, 21, and 13 eyes in groups 1, 2, 3, and 4, respectively, for blue-light stimuli. Interquartile ranges are shown with error bars. *P < 0.05, **P < 0.01. NLP: no light perception, LP: light perception, FFP: faint form perception, FP: form perception, PLR: pupillary light response, RPC: relative pupillary contraction, RP: retinitis pigmentosa. (For interpretation of the references to colour in this figure legend, the reader is referred to the web version of this article.)

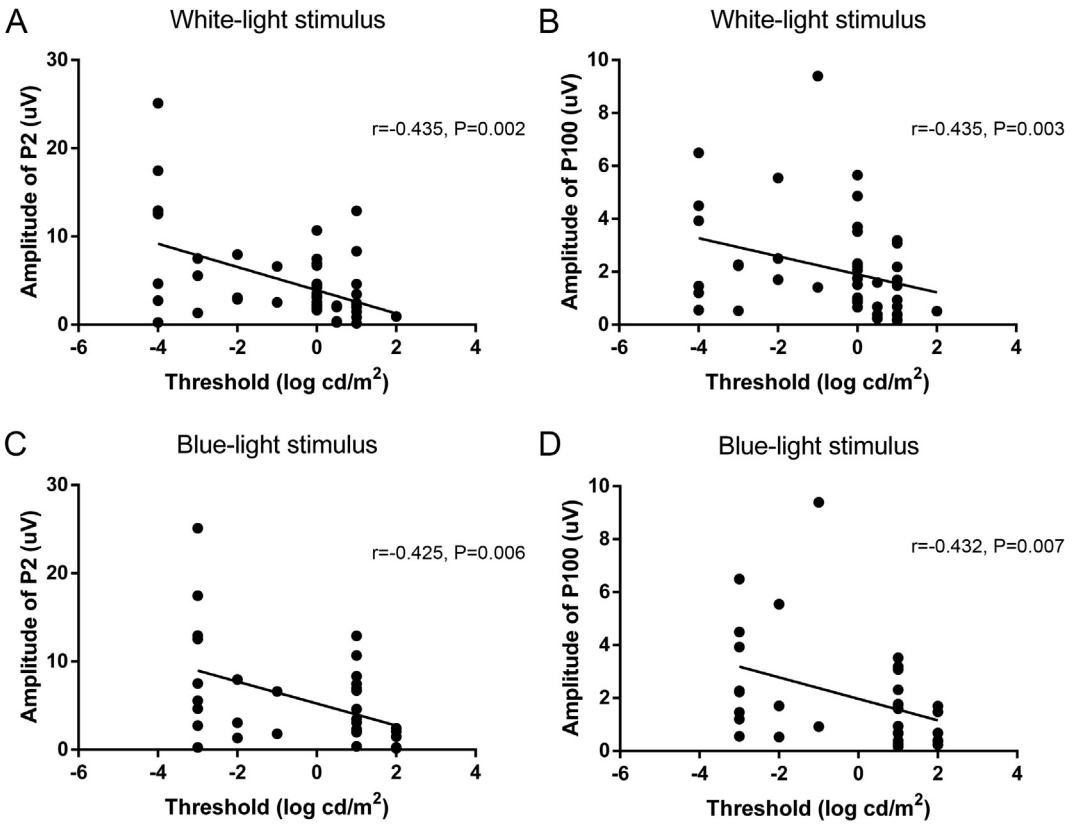

Fig. 6. Correlation between the amplitude of the VEP and the PLR threshold under white-light and blue-light stimuli (scatterplot). Spots in each panel represent the amplitude of each patient with different stimulus thresholds. (A) The correlation between the amplitude of P2 and the PLR threshold under a white-light stimulus (r = −0.435, *P* = 0.002). (B) The correlation between the amplitude of P100 and the PLR threshold under a white-light stimulus (r = −0.435, *P* = 0.003). (C) The correlation between the amplitude of P2 and the PLR threshold under a blue-light stimulus (r = −0.425, *P* = 0.006). (D) The correlation between the amplitude of P2 and the PLR threshold under a blue-light stimulus (r = −0.432, *P* = 0.007). Spearman rank correlation analysis was used. VEP: visual evoked potential, PLR: pupillary light response.

Table 2
Characteristics of the subjects who received fMRI.

Number	Age	Sex	BCVA (OD)	BCVA (OS)
NC1	34	M	1.0	1.0
NC2	29	M	1.2	1.2
NC3	26	M	1.2	1.2
NC4	24	M	1.0	1.0
NC5	33	M	1.0	1.0
PAT1	56	F	NLP	NLP
PAT2	57	M	LP	LP
PAT3	47	M	LP	LP
PAT4	38	F	HM	HM
PAT5	56	F	HM	HM

NLP: no light perception, LP: light perception, HM: hand movement, BCVA: best corrected visual acuity, M: male, F: female, OD: oculus dexter, OS: oculus sinister.

photoreceptors are also affected, leading to severe vision impairment in advanced RP. We found that the OPL and ONL in the NLP patients were thinner than those in the other three groups. After the outer segment of the photoreceptor becomes thinner, the ONL thickness in RP decreases (Eriksson and Alm, 2009; Lazow et al., 2011). It has also been reported that progressive ONL thinning is related to bipolar cell dendritic retraction and amacrine and muller cell reactivity increase (Aleman et al., 2007). However, there was no significant difference in the MRT, GCL-IPL or INL thicknesses among the four RP groups. This finding is consistent with a study that showed a reduction in the thickness of the outer segment and no significant reduction in the total retinal thickness (Wen et al., 2012). This thinning of the outer retina with preservation of the inner retinal layers has been described in many studies (Hood et al., 2009; Vamos et al., 2011). Although the INL thickness was not significantly different among RP patients, we observed that the INL was thicker as the disease progressed. There are several possible reasons for outer retina thinning and inner retina thickening. Some researchers have speculated that Henle fibers are less susceptible to RP-related changes (Curcio et al., 2011). Another report suggested that the edematous retinal nerve fiber layer (RNFL) responds to ONL loss, leading to a comparative preservation of the inner retina (Beltran et al., 2006).

What kind of functional changes will result in the reduction of the outer retina? At the retinal level, our study demonstrated that neither ffERG nor PERG can display visual pathway function differences among patients at the advanced stage of RP, as they result in nonrecordable ERG. In a study that enrolled RP patients with moderate to profound vision loss, ffERG provided some useful information regarding residual visual function (Ayton et al., 2014). The retinal function of RP patients detected by PERG indices improved after subthreshold diode micropulse laser treatment (Luttrull, 2018). Another retrospective cohort also used ffERG, PERG, and mf-ERG to record retinal dysfunction (Errera et al., 2019). mf-ERG is useful for objectively evaluating function in the central part of the retina (Vajaranant et al., 2002), and some researchers believe mf-ERG may still be able to elicit responses so it may be used to track disease progression (Messias et al., 2013). ffERG detects the function of rod cells and reflects the function of the full retinal field (McCulloch et al., 2015; Schroeder and Kjellström, 2018; Verbakel et al., 2018), while PERG and mf-ERG detect the function of cone cells and reflect macular and posterior retinal function. The patients in our study had advanced or end-stage disease that was

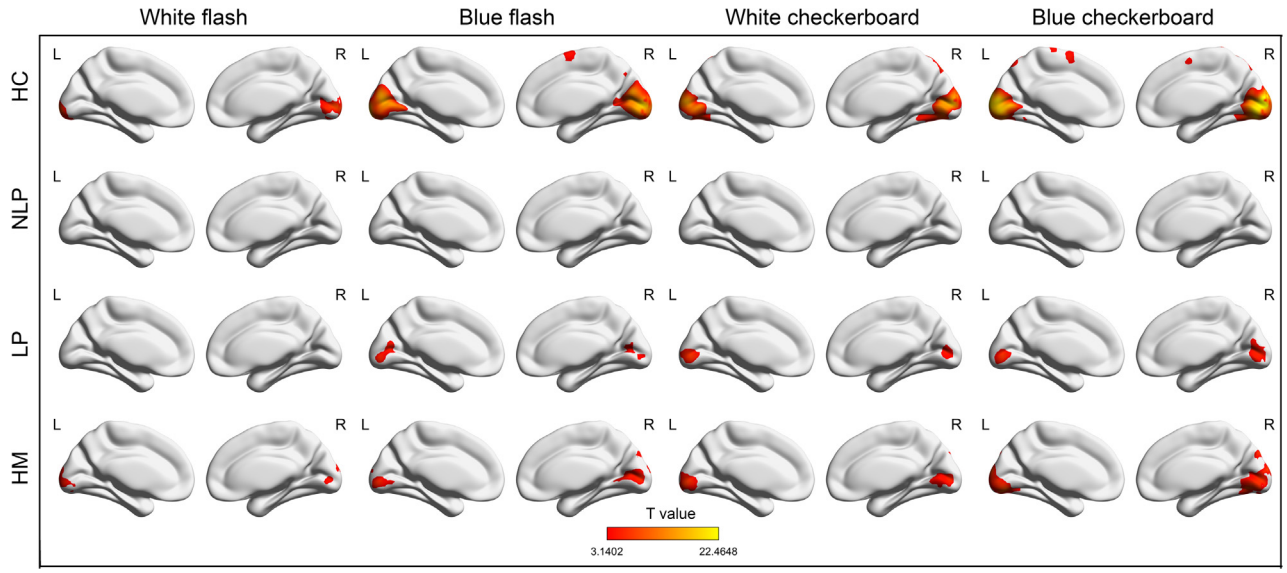

Fig. 7. Statistical activation maps of the visual cortex among the HCs and RP patients under different light stimuli. Peak-level topological false discovery rate correction was used to correct for multiple comparisons under different stimuli conditions among all of the participants. The color bars represent the T values. HC: healthy control, RP: retinitis pigmentosa, NLP: no light perception, LP: light perception, HM: hand movement. (For interpretation of the references to colour in this figure legend, the reader is referred to the web version of this article.)

more severe than the disease of patients included in the above studies. In the advanced stage of RP, most patients become blind, and peripheral retinal function is severely damaged. In blind RP patients, severe macular damage and photoreceptor degeneration are responsible for the nonrecordability of waveforms (Bach et al., 2013; Verbakel et al., 2018; Young et al., 2012).

The VEP response reflects the integrity of the visual pathway (Odom et al., 2016). The VEP pattern is extremely useful for studying optic nerve and postchiasmal function when combined with ERG testing (Holder, 2004). A study to assess the contrast response of the visual system by the VEP found that both the parvocellular (PC) and magnocellular (MC) pathways in RP patients were impaired and that the temporal frequency impacted the impairment degree of the MC pathway (Alexander et al., 2005). Notably, our research illustrates that the VEP is still valid for distinguishing among blind RP patients and that the FVEP is more effective in observing differences than the PVEP. In our study, the number of residual photoreceptor cells in RP patients with bare LP or NLP was less than that in patients with FP. A smaller number of residual photoreceptors had less ability to convert optical stimulation to an electrical signal, leading to a lower amplitude of the VEP. Because blind RP patients are still partially aware of the presence of light even without the ability to identify images, it is reasonable that the FVEP is more useful for evaluating visual pathway function.

The PLR is a significant nonimaging visual response that constricts the pupil in answer to increased illumination. The signal input for this reflex originates from rod and cone photoreceptors and intrinsically photosensitive retinal ganglion cells (Hattar et al., 2003). We used both blue- and white-light stimuli to examine RP patients' visual function. We found that even among blind RP patients, patients with different grades had different PLR thresholds. This result is consistent with our results showing the ONL thickness and the FVEP P2 amplitude; NLP and LP patients had higher thresholds than people with FP, although the difference was minor. We know that low-intensity blue light mainly evokes a rod-mediated pupillary response, while the transient and sustained pupillary responses to high-intensity blue light most likely result from a combination of cone and melanopsin activation (Kardon et al., 2009). Therefore, the varying quantities of residual photoreceptors can be interpreted as resulting in the various thresholds. The negative correlation between the threshold of the PLR and the amplitude of the VEP provided strong evidence for their effectiveness for assessing visual function in blindness.

As the VEP and PLR showed differences, it is interesting to explore whether the visual pathway function in the cortex differs among these patients, and fMRI is an appropriate tool for assessing visual cortex function. Our laboratory's previous research results showed differences in visual cortex area activation and functional connectivity in amblyopia patients (Liang et al., 2017; Wang et al., 2017). In this study, we used blue- and white-light stimuli to explore visual cortex activation in both RP patients and normal participants, and we found that some types of stimulation could activate the visual cortex of RP patients. However, we cannot determine who had stronger activation because of the small number of cases; no statistical analyses were performed. A previous study revealed that resting-state functional connectivity in RP is lower than normal and that the synchronicity of neural activity changes in the primary visual area is reduced in RP individuals (Dan et al., 2019). A study showed significantly decreased gray matter volume (GMV) in V1 in RP individuals, and these decreased GMV values were closely linked to the degree of visual field deficit (Rita Machado et al., 2017). Moreover, a fMRI study found that patients with stronger V1 BOLD responses had less severe impairment of contrast sensitivity (Castaldi et al., 2019), which is similar to our study. The activation of V1, which is anatomically identical to Brodmann's area 17, could be an objective indicator to evaluate residual visual function of the blind. A previous report published in 2016 evaluated seven blind RP subjects by fMRI and found that BOLD responses to visual input were enhanced after the prolonged use of Argus II retinal prosthesis (Castaldi et al., 2016). In the future, this tool could be used to predict patient prognosis and the restoration degree of clinical treatments for blindness associated with RP. There are some limitations of our present fMRI research, and we can demonstrate only that with this technique, both the patients and normal participants had activation of the visual cortex, especially in V1. Therefore, it is necessary to explore the differences among blind RP patients in studies with larger sample sizes in the future.

5. Conclusions

Despite the difficulty of assessing visual pathway function in blind RP patients, our study provides evidence that OCT, VEP, PLR and fMRI assessments can be useful for distinguishing morphological and functional differences among blind RP patients. Even if photoreceptor cell death causes impairment of full retinal function, visual pathway function could be assessed by VEP, PLR and fMRI assessments. The results of these methods can serve as outcomes or predictive measures to potentially evaluate the effects of retinal intervention. Overall, this study provides important evaluation methods that can be applied in future clinical trials.

Declaration of Competing Interest

The authors declare that they have no known competing financial interests or personal relationships that could have appeared to influence the work reported in this paper.

Acknowledgments

We are grateful to Cheng Sun, Sha Li, Linbo He, and Bo Liu for supporting this study in data acquisition. We thank Chen Liu, Xuntao Yin and Liangrui Fang of the Department of Radiology who provided the technique support on fMRI.

This work was supported by the Military Key Program (BWS13C015), the Natural Basic Research Program of China (2018YFA0107301), the National Natural Science Foundation of China (81130017, 81900902, 81974138) and the Natural Science Foundation of Chongqing (cstc2017jcyjAX0111).

References

Aleman TS, Cideciyan AV, Sumaroka A, Schwartz SB, Roman AJ, Windsor EA, et al. Inner retinal abnormalities in X-linked retinitis pigmentosa with RPGR mutations. Invest Ophthalmol Vis Sci 2007;48(10):4759–65.

Alexander KR, Rajagopalan AS, Seiple W, Zemon VM, Fishman GA. Contrast response properties of magnocellular and parvocellular pathways in retinitis pigmentosa assessed by the visual evoked potential. Invest Ophthalmol Vis Sci 2005;46 (8):2967–73.

Amaro Jr E, Barker GJ. Study design in fMRI: basic principles. Brain Cogn 2006;60 (3):220–32.

Ashtari M, Nikonova ES, Marshall KA, Young GJ, Aravand P, Pan W, et al. The role of the human visual cortex in assessment of the long-term durability of retinal gene therapy in follow-on RPE65 clinical trial patients. Ophthalmology 2017;124(6):873–83.

Ayton LN, Apollo NV, Varsamidis M, Dimitrov PN, Guymer RH, Luu CD. Assessing residual visual function in severe vision loss. Invest Ophthalmol Vis Sci 2014;55 (3):1332–8.

Bach M, Brigell MG, Hawlina M, Holder GE, Johnson MA, McCulloch DL, et al. ISCEV standard for clinical pattern electroretinography (PERG): 2012 update. Doc Ophthalmol 2013;126(1):1–7.

Beltran WA, Hammond P, Acland GM, Aguirre GD. A frameshift mutation in RPGR exon ORF15 causes photoreceptor degeneration and inner retina remodeling in a model of X-linked retinitis pigmentosa. Invest Ophthalmol Vis Sci 2006;47 (4):1669–81.

Buxton RB, Griffeth VE, Simon AB, Moradi F, Shmuel A. Variability of the coupling of blood flow and oxygen metabolism responses in the brain: a problem for interpreting BOLD studies but potentially a new window on the underlying neural activity. Front Neurosci 2014;8:139.

Castaldi E, Cicchini GM, Cinelli L, Biagi L, Rizzo S, Morrone MC. Visual BOLD response in late blind subjects with Argus II retinal prosthesis. PLoS Biol 2016;14(10):e1002569.

Castaldi E, Cicchini GM, Falsini B, Binda P, Morrone MC. Residual visual responses in patients with retinitis pigmentosa revealed by functional magnetic resonance imaging. Transl Vis Sci Technol 2019;8(6):44.

Chen W, Zhang L, Xu YG, Zhu K, Luo M. Primary angle-closure glaucomas disturb regional spontaneous brain activity in the visual pathway: an fMRI study. Neuropsychiatr Dis Treat 2017;13:1409–17.

Curcio CA, Messinger JD, Sloan KR, Mitra A, McGwin G, Spaide RF. Human chorioretinal layer thicknesses measured in macula-wide, high-resolution histologic sections. Invest Ophthalmol Vis Sci 2011;52(7):3943–54.

Dan HD, Zhou FQ, Huang X, Xing YQ, Shen Y. Altered intra- and inter-regional functional connectivity of the visual cortex in individuals with peripheral vision loss due to retinitis pigmentosa. Vision Res 2019;159:68–75.

Dias MF, Joo K, Kemp JA, Fialho SL, da Silva Cunha A, Jr., Woo SJ, et al. Molecular genetics and emerging therapies for retinitis pigmentosa: Basic research and clinical perspectives. Prog Retin Eye Res 2018;63:107-31.

Duebel J, Marazova K, Sahel JA. Optogenetics. Curr Opin Ophthalmol 2015;26 (3):226–32.

Eriksson U, Alm A. Macular thickness decreases with age in normal eyes: a study on the macular thickness map protocol in the Stratus OCT. Br J Ophthalmol 2009;93(11):1448–52.

Errera MH, Robson AG, Wong T, Hykin PG, Pal B, Sagoo MS, et al. Unilateral pigmentary retinopathy: a retrospective case series. Acta Ophthalmol 2019;97 (4):e601–17.

Fahim A. Retinitis pigmentosa: recent advances and future directions in diagnosis and management. Curr Opin Pediatr 2018;30(6):725–33.

Finke C, Zimmermann H, Pache F, Oertel FC, Chavarro VS, Kramarenko Y, et al. Association of visual impairment in neuromyelitis optica spectrum disorder with visual network reorganization. JAMA Neurol 2018;75(3):296–303.

Fox PT, Raichle ME. Stimulus rate dependence of regional cerebral blood flow in human striate cortex, demonstrated by positron emission tomography. J Neurophysiol 1984;51(5):1109–20.

Fox PT, Raichle ME. Stimulus rate determines regional brain blood flow in striate cortex. Ann Neurol 1985;17(3):303–5.

Frezzotti P, Giorgio A, Motolese I, De Leucio A, Iester M, Motolese E, et al. Structural and functional brain changes beyond visual system in patients with advanced glaucoma. PLoS One 2014;9(8):e105931.

Hattar S, Lucas RJ, Mrosovsky N, Thompson S, Douglas RH, Hankins MW, et al. Melanopsin and rod-cone photoreceptive systems account for all major accessory visual functions in mice. Nature 2003;424(6944):76–81.

Holder GE. Electrophysiological assessment of optic nerve disease. Eye (Lond) 2004;18(11):1133–43.

Hood DC, Lin CE, Lazow MA, Locke KG, Zhang X, Birch DG. Thickness of receptor and post-receptor retinal layers in patients with retinitis pigmentosa measured with frequency-domain optical coherence tomography. Invest Ophthalmol Vis Sci 2009;50(5):2328–36.

Jolly JK, Bridge H, MacLaren RE. Outcome measures used in ocular gene therapy trials: a scoping review of current practice. Front Pharmacol 2019;10:1076.

Kardon R, Anderson SC, Damarjian TG, Grace EM, Stone E, Kawasaki A. Chromatic pupil responses: preferential activation of the melanopsin-mediated versus outer photoreceptor-mediated pupil light reflex. Ophthalmology 2009;116 (8):1564–73.

Khoury B, Kogan C, Daouk S. International Classification of Diseases 11th Edition (ICD-11). Encyclopedia of Personality and Individual Differences; 2017. p. 1-6.

Klassen H. Stem cells in clinical trials for treatment of retinal degeneration. Expert Opin Biol Ther 2016;16(1):7–14.

Krueger G, Granziera C. The history and role of long duration stimulation in fMRI. Neuroimage 2012;62(2):1051–5.

Lazow MA, Hood DC, Ramachandran R, Burke TR, Wang YZ, Greenstein VC, et al. Transition zones between healthy and diseased retina in choroideremia (CHM) and Stargardt disease (STGD) as compared to retinitis pigmentosa (RP). Invest Ophthalmol Vis Sci 2011;52(13):9581–90.

Liang M, Xie B, Yang H, Yin X, Wang H, Yu L, et al. Altered interhemispheric functional connectivity in patients with anisometropic and strabismic amblyopia: a resting-state fMRI study. Neuroradiology 2017;59(5):517–24.

Liu Y, Chen SJ, Li SY, Qu LH, Meng XH, Wang Y, et al. Long-term safety of human retinal progenitor cell transplantation in retinitis pigmentosa patients. Stem Cell Res Ther 2017;8(1):209.

Logothetis NK. What we can do and what we cannot do with fMRI. Nature 2008;453 (7197):869–78.

Luo YH, da Cruz L. The Argus(®) II Retinal Prosthesis System. Prog Retin Eye Res 2016;50:89–107.

Luttrull JK. Improved retinal and visual function following panmacular subthreshold diode micropulse laser for retinitis pigmentosa. Eye (Lond) 2018;32(6):1099–110.

Maguire AM, Russell S, Wellman JA, Chung DC, Yu ZF, Tillman A, et al. Efficacy, safety, and durability of voretigene neparvovec-rzyl in RPE65 mutation-associated inherited retinal dystrophy: results of phase 1 and 3 trials. Ophthalmology 2019;126(9):1273–85.

Masamoto K, Vazquez A, Wang P, Kim SG. Trial-by-trial relationship between neural activity, oxygen consumption, and blood flow responses. Neuroimage 2008;40 (2):442–50.

Masuda Y, Horiguchi H, Dumoulin SO, Furuta A, Miyauchi S, Nakadomari S, et al. Task-dependent V1 responses in human retinitis pigmentosa. Invest Ophthalmol Vis Sci 2010;51(10):5356–64.

McCulloch DL, Marmor MF, Brigell MG, Hamilton R, Holder GE, Tzekov R, et al. Erratum to: ISCEV Standard for full-field clinical electroretinography (2015 update). Doc Ophthalmol 2015;131(1):81–3.

Messias K, Jagle H, Saran R, Ruppert AD, Siqueira R, Jorge R, et al. Psychophysically determined full-field stimulus thresholds (FST) in retinitis pigmentosa: relationships with electroretinography and visual field outcomes. Doc Ophthalmol 2013;127(2):123–9.

Miraldi Utz V, Coussa RG, Antaki F, Traboulsi EI. Gene therapy for RPE65-related retinal disease. Ophthalmic Genet 2018;39(6):671–7.

Odom JV, Bach M, Brigell M, Holder GE, McCulloch DL, Mizota A, et al. ISCEV standard for clinical visual evoked potentials: (2016 update). Doc Ophthalmol 2016;133(1):1–9.

Ogawa S, Lee TM, Nayak AS, Glynn P. Oxygenation-sensitive contrast in magnetic resonance image of rodent brain at high magnetic fields. Magn Reson Med 1990;14(1):68–78.
Rachitskaya AV, Yuan A. Argus II retinal prosthesis system: An update. Ophthalmic Genet 2016;37(3):260–6.
Rita Machado A, Carvalho Pereira A, Ferreira F, Ferreira S, Quendera B, Silva E, et al. Structure-function correlations in Retinitis Pigmentosa patients with partially preserved vision: a voxel-based morphometry study. Sci Rep 2017;7(1):11411.
Rosen BR, Savoy RL. fMRI at 20: has it changed the world?. Neuroimage 2012;62(2):1316–24.
Russell S, Bennett J, Wellman JA, Chung DC, Yu Z-F, Tillman A, et al. Efficacy and safety of voretigene neparvovec (AAV2-hRPE65v2) in patients with RPE65 -mediated inherited retinal dystrophy: a randomised, controlled, open-label, phase 3 trial. Lancet 2017;390(10097):849–60.
Schroeder M, Kjellström U. Full-field ERG as a predictor of the natural course of ABCA4-associated retinal degenerations. Mol Vis 2018;24:1–16.
Spitschan M, Datta R, Stern AM, Brainard DH, Aguirre GK. Human visual cortex responses to rapid cone and melanopsin-directed flicker. J Neurosci 2016;36(5):1471–82.
Thomas CG, Menon RS. Amplitude response and stimulus presentation frequency response of human primary visual cortex using BOLD EPI at 4 T. Magn Reson Med 1998;40(2):203–9.
Vajaranant TS, Seiple W, Szlyk JP, Fishman GA. Detection using the multifocal electroretinogram of mosaic retinal dysfunction in carriers of X-linked retinitis pigmentosa. Ophthalmology 2002;109(3):560–8.
Vamos R, Tatrai E, Nemeth J, Holder GE, DeBuc DC, Somfai GM. The structure and function of the macula in patients with advanced retinitis pigmentosa. Invest Ophthalmol Vis Sci 2011;52(11):8425–32.
Verbakel SK, van Huet RAC, Boon CJF, den Hollander AI, Collin RWJ, Klaver CCW, et al. Non-syndromic retinitis pigmentosa. Prog Retin Eye Res 2018;66:157–86.
Wang H, Crewther SG, Liang M, Laycock R, Yu T, Alexander B, et al. Impaired activation of visual attention network for motion salience is accompanied by reduced functional connectivity between frontal eye fields and visual cortex in strabismic amblyopia. Front Hum Neurosci 2017;11:195.
Wang X, Cui D, Zheng L, Yang X, Yang H, Zeng J. Combination of blood oxygen level-dependent functional magnetic resonance imaging and visual evoked potential recordings for abnormal visual cortex in two types of amblyopia. Mol Vis 2012;18:909–19.
Wen Y, Klein M, Hood DC, Birch DG. Relationships among multifocal electroretinogram amplitude, visual field sensitivity, and SD-OCT receptor layer thicknesses in patients with retinitis pigmentosa. Invest Ophthalmol Vis Sci 2012;53(2):833–40.
Yan CG, Wang XD, Zuo XN, Zang YF. DPABI: data processing & analysis for (resting-state) brain imaging. Neuroinformatics 2016;14(3):339–51.
Yoshida M, Origuchi M, Urayama S, Takatsuki A, Kan S, Aso T, et al. fMRI evidence of improved visual function in patients with progressive retinitis pigmentosa by eye-movement training. Neuroimage Clin 2014;5:161–8.
You Y, Joseph C, Wang C, Gupta V, Liu S, Yiannikas C, et al. Demyelination precedes axonal loss in the transneuronal spread of human neurodegenerative disease. Brain 2019;142(2):426–42.
Young B, Eggenberger E, Kaufman D. Current electrophysiology in ophthalmology: a review. Curr Opin Ophthalmol 2012;23(6):497–505.